Article

Relativistic Multiconfigurational *Ab Initio* Calculation of Uranyl 3d4f Resonant Inelastic X-ray Scattering

Robert Polly,* Bianca Schacherl, Jörg Rothe, and Tonya Vitova

Read Online

ACCESS | Metrics & More | Article Recommendations

ABSTRACT: We applied relativistic multiconfigurational all-electron *ab initio* calculations including the spin−orbit interaction to calculate the 3d4f resonant inelastic X-ray scattering (RIXS) map ($3d_{3/2} \rightarrow 5f_{5/2}$ U M_4 absorption edge and $4f_{5/2} \rightarrow 3d_{3/2}$ U M_β emission) of uranyl (UO_2^{2+}). The calculated data are in excellent agreement with experimental results and allow a detailed understanding of the observed features and an unambiguous assignment of all involved intermediate and final states. The energies corresponding to the maxima of the resonant emission and the non-resonant (normal) emission were determined with high accuracy, and the corresponding X-ray absorption near edge structure spectra extracted at these two positions were simulated and agree well with the measured data. With the high quality of our theoretical data, we show that the cause of the splitting of the three main peaks in emission is due to the fine structure splitting of the 4f orbitals induced through the trans di-oxo bonds in uranyl and that we are able to obtain direct information about the energy differences between the 5f and 4f orbitals: $\Delta 5f\ \delta/\phi - 4f\ \delta/\phi$, $\Delta 5f\ \pi^* - 4f\ \pi$, and $\Delta 5f\ \sigma^* - 4f\ \sigma$ from the 3d4f RIXS map. RIXS maps contain a wealth of information, and *ab initio* calculations facilitate an understanding of their complex structure in a clear and transparent way. With these calculations, we show that the multiconfigurational protocol, which is nowadays applied as a standard tool to study the X-ray spectra of transition metal complexes, can be extended to the calculation of RIXS maps of systems containing actinides.
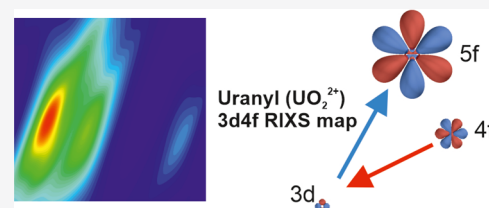
1. INTRODUCTION

The thorough understanding of the electronic structure of actinides (An) and the often puzzling contribution of the 5f orbitals to chemical bonding are of major interest in chemistry.[1] The electronic structure is best probed by combining X-ray spectroscopy with relativistic multiconfigurational *ab initio* calculations.[2−4] Advanced spectroscopic techniques of An, such as An $M_{4,5}$ absorption edge high-energy resolution X-ray absorption near edge structure (HR-XANES)[5−10] and 3d4f resonant inelastic X-ray scattering (RIXS),[11−14] are bulk-sensitive techniques, which can be applied *in situ*. An improved understanding of the An interaction with the constituents of the geo- and ecosphere is highly relevant for the reliable safety assessment of nuclear waste disposals and of An behavior in the environment,[15−19] and X-ray spectroscopy together with *ab initio* calculations is an effective tool for this purpose.[20]

Vitova et al.[2] published M_4 HR-XANES ($3d_{3/2} \rightarrow 5f_{5/2}$ U M_4 absorption edge) and 3d4f RIXS map (U M_4 absorption edge, $4f_{5/2} \rightarrow 3d_{3/2}$ U M_β emission) spectra of uranyl (UO_2^{2+}) with uranium in its hexavalent oxidation state U(VI) with a superior energy resolution. These spectra clearly resolve three pronounced peaks (see Figure 3a,d in ref 2). They can be attributed to excitations into nonbonding 5f δ/ϕ and antibonding 5f π^* and 5f σ^* orbitals of uranyl (σ, π, δ, and ϕ designate the rotational symmetry with respect to the molecular axis in the $D_{\infty h}$ point group symmetry). The 3d4f RIXS map governed by the Kramers−Heisenberg formalism[11,21−24] is

based on a 2D representation of X-ray fluorescence emission measured as a function of the excitation energy and gives further valuable information beyond the HR-XANES spectra.

During the past decade, the research field of computational X-ray spectroscopy has witnessed an enormous advancement.[4,24−43] The studies either utilize multiconfigurational *ab initio* methods,[29−36] density functional theory (DFT)-based restricted open-shell configuration interaction singles (ROCIS),[24,37−40] pair natural orbital-restricted open-shell configuration interaction (PNO-ROCIS),[41] or multireference methods such as multireference configuration interaction (MRCI) or multireference equation of motion coupled cluster (MR-EOM-CC).[42,43]

The progress in relativistic multiconfigurational *ab initio* methods including static and dynamic electron correlation, scalar relativistic effects, and spin−orbit coupling (SOC)[44−55] now permits precise electronic structure calculations of An systems[3] with core-electrons excited to nonbonding or antibonding orbitals or to the continuum. There are many
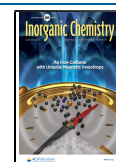
studies investigating the RIXS spectra of transition metals by applying multiconfigurational methods,[30−36] DFT- or PNO-ROCIS,[24,37−40] MRCI, or MR-EOM-CC.[43] The application of *ab initio* methods to X-ray spectroscopy of An is scarce.[3,56] Sergentu et al.[3] presented relativistic multiconfigurational calculations of HR-XANES, reproducing the HR-XANES spectra of Vitova et al.[2] to a high accuracy. Alternatively, X-ray spectra and RIXS maps of transition metals and An are calculated using semiempirical approaches, such as the ligand-field multiplet semiempirical method,[57−61] the charge-transfer multiplet method,[62,63] or the crystal-field multiplet theory.[58,59,62,64,65]

The main goal of this work is to show that relativistic multiconfigurational *ab initio* calculation of RIXS spectra can be applied to challenging chemical systems involving An ions to provide accurate results and reproduce the multiplet structure of the spectra. The calculations help us understand a complex RIXS map of An systems in a clear and transparent way. The results of our calculations allow us to answer several open questions concerning some features of the 3d4f RIXS map observed by Vitova et al.:[2]

(1) clarification of why the two peaks attributed to the excitation into 5f π^* and 5f σ^* are slightly red-shifted (to lower energy) in emission compared to the 5f δ/ϕ peak,

(2) explanation of why the maxima of the resonant and the non-resonant (normal) emissions of the RIXS map do not coincide, and

(3) understanding why the HR-XANES spectra measured by positioning the X-ray emission spectrometer at the maximum of the resonant or non-resonant (normal) emission line differ only slightly.

These calculations are, to our knowledge, the first application of relativistic multiconfigurational *ab initio* methods to RIXS maps of An systems.

2. METHODS

An compounds have in many cases states with a pronounced multiconfigurational character. This is even more severe for the excited states of such systems.[66,67] The ground state of uranyl is a closed-shell single reference state, but the open-shell exited states relevant for our investigation cannot be described by a single configuration. They have a pronounced multiconfigurational character.

Therefore, the methods of choice comprise the complete and restricted active space self-consistent field (CASSCF/RASSCF)[44−48] methods and the corresponding second-order perturbation-theory corrected variants (CASPT2/RASPT2).[49−51,53,54]

We use the approach recently suggested by Sergentu et al.[3] for An. They showed that RASSCF/RASPT2 calculations followed by the inclusion of the SOC, by calculating the interaction of scalar relativistic spin states (L−S) via a mean-field SO operator,[55] provide accurate results for HR-XANES $M_{4,5}$ spectra of An and properly account for the multiplet structure of the spectra.

In the crystal-field multiplet theory,[58,59,62,64,65] the local model requires the description of all the energy contributions including H_{SO} (SO interaction) and the crystal-field multiplet Hamiltonian HCF (e.g., refer to Zimmermann et al.[68]). They are all naturally included in our *ab initio* approach as outlined above.

MS-RASPT2[51] calculations were performed for the U M_4 absorption edge HR-XANES and 3d4f RIXS calculation with the IPEA shift of 0 E_h and an imaginary shift of 0.2 E_h. All calculations were all-electron calculations in the C_i symmetry at the bond length of 176 pm.[2,3] The molecular axis is oriented in the z-direction. We reduced the symmetry from $D_{\infty h}$ to C_i, although the largest Abelian subgroup of $D_{\infty h}$ is D_{2h}. However, performing the calculations in C_i is preferable since the 3d (A_g) and 4f/5f (A_u) orbitals are in separate irreducible representations.

There are several more advantages, such as the RAS1 and RAS3 orbitals being in different irreducible representations and all the 3d, 4f, and 5f orbitals being optimized together in one irreducible representation. Test calculations supported this choice. Scalar relativistic effects were included by using a second-order Douglas−Kroll−Hess Hamiltonian in combination with a relativistic atomic natural orbital basis set (ANO-VQZ).[69,70] The SOC is treated by the interaction of scalar relativistic spin states via a mean-field SO operator using RASSI.[55] All the calculations were performed on an isolated uranyl ion because Sergentu et al.[3] showed that the calculated HR-XANES spectra for plutonyl (PuO_2^{2+}) are almost identical with or without water molecules in the equatorial plane included in the calculations. We used MOLCAS8.4[71] for the calculations.

For an easier understanding of the following discussion regarding the choices of the active spaces in the HR-XANES and RIXS calculations, the molecular orbital (MO) diagram of uranyl including the relevant orbitals is shown in Figure 1.
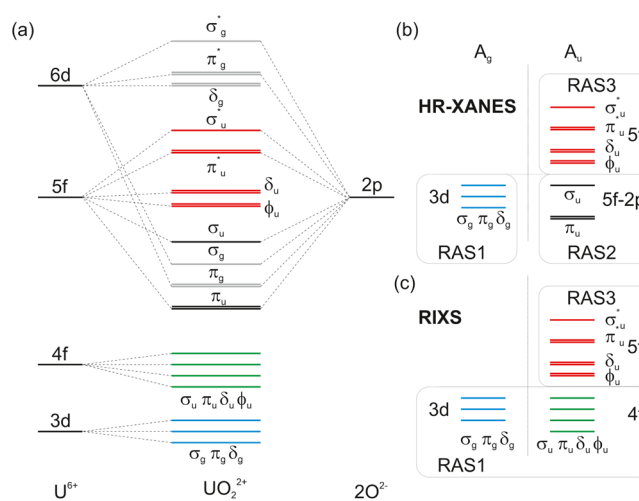

Figure 1. Qualitative MO diagram for the relevant orbitals of uranyl and selection of the active spaces for the HR-XANES and RIXS calculations. The bonding orbitals formed by covalent mixing of 5f and 6d of uranium and 2p of oxygen are shown in black and gray. The 3d and 4f core orbitals of uranium are shown in blue and green, respectively, together with their correct labeling as MOs of uranyl in the $D_{\infty h}$ symmetry. The nonbonding and antibonding orbitals involving 5f are shown in red, and the nonbonding and antibonding orbitals formed with 6d orbitals are shown in gray. (a) MO diagram. (b,c) Active space selection for HR-XANES and RIXS calculations. The orbitals of the RAS1, RAS2, and RAS3 active spaces in the two irreducible representations of C_i (A_g and A_u) are shown.

The uranyl is formed by U^{6+} ($1s^22s^22p^63s^23p^63d^{10}4s^24p^64d^{10}4f^{14}5s^25p^65d^{10}6s^26p^6$) and $2O^{2-}$ ($1s^22s^22p^6$). The bonds are formed between the 5f orbital of uranium and the 2p orbitals of oxygen (σ_u and π_u) and the 6d and the 2p orbitals (σ_g and π_g), resulting in six bonding orbitals (indicated as gray and black lines in Figure 1a). They are occupied by the 12 2p valence electrons of the two oxygen ions. Additionally, there are several unoccupied orbitals, four nonbonding orbitals from the 5f orbitals (δ_u and ϕ_u, shown as red lines in Figure 1a and denoted 5f δ and 5f ϕ, respectively), three antibonding orbitals from the 5f−2p orbitals (π_u^* and σ_u^*, shown as red lines in Figure 1a and denoted 5f π^* and 5f σ^*, respectively), two nonbonding orbitals from the 6d orbitals (δ_g, shown as gray lines in Figure 1a), and three antibonding orbitals from the 6d−2p orbitals (π_g^* and σ_g^*, shown as gray lines in Figure 1a). The 3d and 4f core orbitals of uranium are shown in blue and green and are denoted as 3d $\sigma/\pi/\delta$ and 4f $\sigma/\pi/\delta/\phi$, respectively.

The practical limit for active spaces in CASSCF calculations is 16 electrons in 16 orbitals. For an accurate CASSCF calculation of the uranyl ground state, we need six 2p orbitals of oxygen, seven 5f orbitals

(indicated as red lines in Figure 1a), and three 6d orbitals (omitting the two highlying nonbonding δ_g orbitals) of uranium,[a] totaling 16 orbitals in the active space. They are filled by 12 2p electrons (see refs 66 and 67) of the two oxygen ions. With this, we are already close to the limit. For the calculation of the HR-XANES ($3d_{3/2} \rightarrow 5f_{5/2}$ U M$_4$ absorption edge) and 3d4f RIXS map (U M$_4$ absorption edge and $4f_{5/2} \rightarrow 3d_{3/2}$ U M$_\beta$ emission), several more orbitals (3d and 4f) would be required in the active space of a CASSCF calculation. Therefore, we restrict ourselves to a minimal active space without the six bonding orbitals of oxygen and the three 6d orbitals of uranium and employ the RASSCF method.

2.1. Choice of the Active Spaces for the U M$_4$ Absorption Edge HR-XANES Calculations. Figure 2 gives a schematic
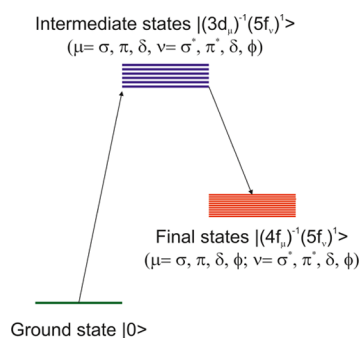

Figure 2. Schematic representation of the HR-XANES and 3d4f RIXS process in uranyl showing the involved states and their respective electronic configurations. The excitations are from the ground state of uranyl to the intermediate states with the electronic configurations $|(3d\,\mu)^{-1}(5f\nu)^1\rangle$ ($\mu = \sigma, \pi, \delta$ and $\nu = \sigma^*, \pi^*, \delta, \phi$). They have one hole in the 3d μ core orbital and one 5f ν valence orbital occupied. The emission if from the intermediate-to-final state transition by filling the hole in the 3d core orbital by an electron from the 4f core orbital, leaving one hole in the 4f μ core orbitals with the final configurations $|(4f\,\mu)^{-1}(5f\nu)^1\rangle$ ($\mu = \sigma, \pi, \delta, \phi$ and $\nu = \sigma^*, \pi^*, \delta, \phi$).

representation of the HR-XANES and 3d4f RIXS process in uranyl with the involved states and their respective electronic configurations. Figure 3 presents a qualitative MO diagram and the electronic configurations of the intermediate and final states of the RIXS process. Here and in the following, it should be stressed that the intermediate state of the RIXS process is the final state of the HR-XANES excitation.

The states required to determine all observed excitation energies of the HR-XANES spectra ($3d_{3/2} \rightarrow 5f_{5/2}$ U M$_4$ absorption edge) have $3d^{10}4f^{14}5f^0$ and $3d^94f^{14}5f^1$ (one hole in the 3d shell) orbital occupations (see Figures 2 and 3a). We introduce the notation $|(3d\,\sigma)^{-1}(5f\,\sigma)^1\rangle$ for a state with a hole in the 3d σ orbitals and one electron occupying a 5f σ^* orbital and $|(3d)^{-1}(5f)^1\rangle$ for a state with a hole in an unspecified 3d orbital and one electron occupying any 5f orbital. The relevant excited spin-free states for the HR-XANES calculations have the electronic configurations $|(3d\,\mu)^{-1}(5f\,\nu)^1\rangle$ ($\mu = \sigma, \pi, \delta$ and $\nu = \sigma^*, \pi^*, \delta, \phi$) (see Figures 2 and 3a) with one electron occupying a nonbonding or antibonding orbital involving 5f (shown in red in Figures 1 and 3a) and a hole in a 3d or 4f core orbital (shown in blue and green in Figures 1 and 3a). The corresponding singlet and triplet states (35 each) are $^{1,3}\Sigma_u$ (5), $^{1,3}\Pi_u$ (10), $^{1,3}\Delta_u$ (8), $^{1,3}\Phi_u$ (6), $^{1,3}\Gamma_u$ (4), and $^{1,3}H_u$ (2) (the number of states is given in brackets). These states are split by the differences in the spin and spatial orientations of the electrons, here referred to as multiplet splittings. They correspond to one-electron core excitations with singlet and triplet multiplicities. Including the SOC, these excited states span the whole space of all possible core–hole multiplets, giving rise to the U M$_4$ absorption edge peaks.

The active spaces for the HR-XANES calculations described below are shown in Figure 1b. The five 3d (A$_g$ in C$_i$ symmetry) orbitals (shown as blue lines in Figure 1b) form the RAS1 active space and the seven 5f (A$_u$ in C$_i$ symmetry) orbitals (shown as red lines in Figure 1b) are placed in the RAS3 active space (denoted 3d/5f), allowing two holes in
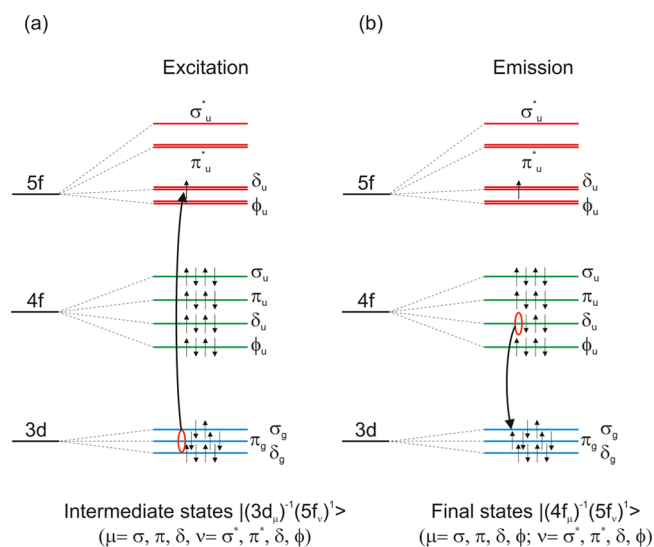
Figure 3. Qualitative MO diagram showing the electronic configurations in the intermediate and final states of the 3d4f RIXS process of uranyl together with the excitation and emission scheme of the HR-XANES and RIXS processes. Only the relevant 3d and 4f core orbitals and the nonbonding and antibonding orbitals formed by the 5f valence orbitals are included (see Figure 1 as well). (a) Intermediate state of the RIXS process with the electronic configurations $|(3d\,\mu)^{-1}(5f\,\nu)^1\rangle$ ($\mu = \sigma, \pi, \delta$ and $\nu = \sigma^*, \pi^*, \delta, \phi$). In the excitation process, a hole in the 3d μ core orbitals is created, and a nonbonding or antibonding orbital of uranyl with contributions of the 5f ν orbital is occupied in the intermediate state. (b) Final state of the RIXS process with the electronic configurations $|(4f\,\mu)^{-1}(5f\,\nu)^1\rangle$ ($\mu = \sigma, \pi, \delta, \phi$ and $\nu = \sigma^*, \pi^*, \delta, \phi$). In the emission process, the hole in the 3d core orbitals is filled by an electron from the 4f μ core orbital, and a hole in the 4f μ orbital remains in the final state.

RAS1 and two electrons in RAS3. We kept the six bonding $\sigma_{g,u}$ and $\pi_{g,u}$ orbitals (shown as gray and black lines in Figure 1a) in the inactive space and the three 6d orbitals in the virtual orbital space (shown as gray lines in Figure 1a). There are 10 active electrons in 12 active orbitals in this minimal active space.

The calculations are complemented by calculations with additional one bonding σ_u and two π_u orbitals (shown as black lines in Figure 1b) in the RAS2 active space (denoted 3d $\sigma_u\pi_u$/5f). These orbitals are covalent bonds formed by 5f σ/π and 2p. The other three bonding σ_g and π_g orbitals (describing 6d−2p bonds and shown as gray lines in Figure 1a) remain in the inactive space. The 3d $\sigma_u\pi_u$/5f active space serves to test the influence of the inclusion of some bonding orbitals on the calculated transition energies. Allowing two electron excitations from RAS1/RAS2 into RAS3 results already in 770 singlet and 1085 triplet states. The RASSCF calculation with an empty RAS2 space (3d/5f) corresponds to an SDCI calculation and the calculation with three bonding orbitals in RAS2 (3d $\sigma_u\pi_u$/5f) to an MR-SDCI calculation.[72] The same active spaces were employed by Sergentu et al.[3] and proven to provide accurate results for uranyl.

2.2. Choice of the Active Spaces for the 3d4f RIXS Calculations. From the discussion above, it is clear for the calculations on the 3d4f RIXS map that an active space beyond the 3d, 4f, and 5f orbitals is not feasible at all.

For the calculation of the 3d4f RIXS map ($3d_{3/2} \rightarrow 5f_{5/2}$ U M$_4$ absorption edge and $4f_{5/2} \rightarrow 3d_{3/2}$ U M$_\beta$ emission), the calculations of the energies of the excited states with occupations $3d^94f^{14}5f^1$ and $3d^{10}4f^{13}5f^1$ are required (see Figures 2 and 3b). The final states of the 3d4f RIXS process have the electronic configurations $|(4f\,\mu)^{-1}(5f\,\nu)^1\rangle$ ($\mu = \sigma, \pi, \delta, \phi$ and $\nu = \sigma^*, \pi^*, \delta, \phi$) (see Figures 2 and 3b). The corresponding singlet and triplet states (49 each) are $^{1,3}\Sigma_g$ (7), $^{1,3}\Pi_g$ (12), $^{1,3}\Delta_g$ (10), $^{1,3}\Phi_g$ (8), $^{1,3}\Gamma_g$ (6), $^{1,3}H_g$ (4), and $^{1,3}I_g$ (2) (the number of states is given in brackets). As for the U M$_4$ absorption edge HR-

XANES calculation, these excited spin-free states are used for the SOC calculation.

The active spaces for the RIXS calculations described below are shown in Figure 1c. The 3d (A_g) orbitals (shown as blue lines in Figure 1c) and the 4f (A_u) orbitals (shown as green lines in Figure 1c) form the RAS1 active space, and the 5f (A_u) orbitals (shown as red lines in Figure 1c) are placed into the RAS3 active space. We have in total 19 active orbitals occupied by 24 electrons. We allowed two holes in the RAS1 space either in A_g or A_u, with two electrons occupying the RAS3 space, corresponding to an SDCI calculation.

The 3d4f RIXS map can be separated into two parts. The resonant emission requires the calculation of the $3d_{3/2} \rightarrow 5f_{5/2}$ and $4f_{5/2} \rightarrow 3d_{3/2}$ transitions of UO_2^{2+}. The non-resonant (normal) emission corresponds to the $4f_{5/2} \rightarrow 3d_{3/2}$ transitions of UO_2^{3+} with the 5f orbitals completely unoccupied.

2.3. Kramers–Heisenberg Formula. The experimental 3d4f RIXS maps spectra of uranyl were obtained for U(VI) in an aqueous solution. Therefore, we employed the approach developed by Maganas et al.[24] for molecules. The resonance scattering cross-section is averaged over all orientations of the molecule and integrated over all directions and polarizations of the scattered radiation.

The calculation of the 3d4f RIXS map is based on the Kramers–Heisenberg (see eqs 1 and 2)[11,21,22,24,30,31] expression. The relevant electronic energies and the corresponding complex transition dipole moments[73] of UO_2^{2+} are used to calculate the RIXS spectra. Estimates for the lifetime broadenings Γ_i and Γ_f are derived from Vitova et al.[2] and adjusted to fit the experimental data.

The calculated electronic energies of all the relevant states of UO_2^{2+} plus the corresponding transition dipole moments[73] are used to calculate the RIXS spectra using the Kramers–Heisenberg formula.[11,21,22,24,30,31] The polarizability tensor reads[24]

$$|\alpha_{\rho\lambda}(E_{ex}, E_{em})|^2 = \sum_f \left| \sum_i \frac{\langle f|\hat{\mu}_\rho|i\rangle\langle i|\hat{\mu}_\lambda|0\rangle}{E_i - E_0 - E_{ex} - i\frac{1}{2}\Gamma_i} \right|^2 \cdot$$
$$\left\{ \frac{\Gamma_f}{(E_f - E_0 - E_{ex} + E_{em})^2 + \frac{1}{4}\Gamma_f^2} \right\} \quad (\rho, \lambda = x, y, z) \tag{1}$$

with the resonance scattering cross-section as follows

$$\sigma_{RIXS}^{total}(E_{ex}, E_{em}) = \frac{8\pi E_{em}^3 E_{ex}}{9c^4} \sum_{\rho,\lambda=x,y,z} |(\alpha_{\rho\lambda}(E_{ex}, E_{em})|^2 \tag{2}$$

μ, $\rho = x, y, z$: (x, y, z) component of the electric−dipole transition operator; $|0\rangle$, E_0: ground state ($3d^{10}4f^{14}5f^0$) and corresponding energy; $|i\rangle$, E_i: intermediate states ($3d^9 4f^{14} 5f^1$) and corresponding energy; $|f\rangle$, E_f: final states ($3d^{10}4f^{13}5f^1$) and corresponding energy; E_{ex}: excitation energy, $E_{ex} = E_i - E_0$; E_{em}: emission energy, $E_{ex} = E_i - E_f$; Γ_i: line broadening due to the lifetime of the intermediate states; and Γ_f: line broadening due to the lifetime of the final states.

If only contributions from direct excitation $|0\rangle \rightarrow |i\rangle$ involving just one intermediate state to the RIXS signal are considered, eq 1 reduces to[24]

$$|\alpha_{\rho\lambda}(E_{ex}, E_{em}, i)|_{resonant}^2$$
$$= \sum_f |\langle f|\hat{\mu}_\rho|i\rangle|^2 |\langle i|\hat{\mu}_\lambda|0\rangle|^2 \cdot \frac{1}{2\pi} \left\{ \frac{\Gamma_i}{(E_i - E_0 - E_{ex})^2 + \frac{1}{4}\Gamma_i^2} \right\} \cdot$$
$$\left\{ \frac{\Gamma_f}{(E_f - E_0 - E_{ex} + E_{em})^2 + \frac{1}{4}\Gamma_f^2} \right\} \tag{3}$$

If the lifetimes of the intermediate and final state are assumed to be very long, Γ_i and Γ_f become very small, and eq 3 can be rewritten as

$$|\alpha_{\rho\lambda}(E_{ex}, E_{em})|_{resonant}^2$$
$$= \sum_i \sum_f |\langle f|\hat{\mu}_\rho|i\rangle|^2 |\langle i|\hat{\mu}_\lambda|0\rangle|^2 \cdot \delta(E_i - E_0 - E_{ex}) \cdot$$
$$\delta(E_f - E_0 - E_{ex} + E_{em}) \tag{4}$$

Equation 4 shows that $|\langle f|\hat{\mu}_\rho|i\rangle|^2 |\langle i|\hat{\mu}_\lambda|0\rangle|^2$ is a measure of the contribution of the $|0\rangle \rightarrow |i\rangle \rightarrow |f\rangle$ excitation/emission to the RIXS map, neglecting interferences and lifetimes of the intermediate and final states (shown in Figures 5 and 6). Therefore, this is valuable information for understanding the whole 3d4f RIXS map in an easy and transparent way.

3. RESULTS

M_4 HR-XANES ($3d_{3/2} \rightarrow 5f_{5/2}$ U M_4 absorption edge) and the 3d4f RIXS map (U M_4 absorption edge and $4f_{5/2} \rightarrow 3d_{3/2}$ U M_β emission) probe the $3d_{3/2} \rightarrow 5f_{5/2}$ excitations and $4f_{5/2} \rightarrow 3d_{3/2}$ U M_β emission. The $3d_{3/2}$, $4f_{5/2}$, and $5f_{5/2}$ atomic orbitals characterized by their total angular momentum $j = 3/2$ and $5/2$ are localized at the uranium atom. Thus, these excitations and emissions provide a local probe of the electronic structure.

The usual notation of M_4 absorption edge ($3d_{3/2} \rightarrow 5f_{5/2}$) and 3d4f RIXS map (U M_4 absorption edge and $4f_{5/2} \rightarrow 3d_{3/2}$ U M_β emission) (see e.g. refs 2 3, and 8) employs the atomic spin orbitals of uranium including the total angular momentum j. We make an effort to assign the atomic spin orbitals ($3d_{3/2}$, $4f_{5/2}$, and $5f_{5/2}$) of uranium to spin-free MOs (3d $\sigma\pi\delta$, 4f $\sigma\pi\delta/\phi$, and 5f $\sigma^*\pi^*\delta/\phi$) of uranyl, which are characterized by the projection ($\sigma, \pi, \delta, \phi$) of their angular momentum l on the molecular axis (oriented in the z-direction in our case).

In uranyl, the 5f atomic orbitals contribute to several unoccupied molecular (spin-free) valence orbitals 5f σ^*, 5f π^*, and 5f δ/ϕ (see Figure 1). All these 5f orbitals have orbital angular momentum $l = 3$ but with different components m_l along the z-axis: 5f σ^* $m_l = 0$, 5f π^* $m_l = 1$, 5f δ $m_l = 2$, and 5f ϕ $m_l = 3$. The 5f δ/ϕ orbitals are nonbonding, and the 5f π^* and 5f σ^* orbitals are antibonding orbitals of uranyl. We adopt the same notation for the 3d and 4f orbitals, which are core-like but still show a small splitting due to the presence of the oxygen ions.

The most important feature in the understanding of the M_4 MR-XANES and the 3d4f RIXS map are the splittings of the 3d, 4f, and 5f orbitals in the presence of the oxygen ions of uranyl. The splitting is the largest for the 5f valence orbitals (5f $\phi \approx$ 5f δ < 5f π^* < 5f σ^*, $\Delta E \approx$ several eV)[2,3,8] and decreases significantly for the 4f (4f $\phi \approx$ 4f δ < 4f $\pi \approx$ 4f σ) and 3d (3d δ < 3d $\pi \approx$ 3d σ) core orbitals (see below). The splittings of the two latter core orbitals seem unfamiliar but result from the fact that the electron density of the 4f σ and 3d σ orbitals is highest toward the oxygen ions, and hence, their energy is the highest (see also Figures 1 and 3). The ordering of the other 4f and 3d orbitals follows the same logic, as is well-known from the ligand field splittings of valence orbitals. Usually, HR-XANES and RIXS maps are interpreted based on these spin-free MOs characterized by their orbital angular momentum.

In the calculations of the M_4 HR-XANES and the 3d4f RIXS map, we calculated all required spin-free molecular states. For M_4 HR-XANES, these are the ground state $|0\rangle$ (A_g symmetry) of UO_2^{2+} and the excited states (A_u symmetry) with singlet and triplet spins. We have for the singlet and triplet states five possible holes in the 3d shell and seven possible 5f orbitals to be occupied, hence providing in total 35 states. The calculation of the RIXS map requires additional singlet and triplet states in A_g symmetry, 49 states each, with seven possible holes in the 4f shell

and seven possible occupations of the 5f orbitals (e.g., $|(4f \sigma)^{-1}(5f \sigma^*)^1\rangle$).

On top of this, SOC is included to determine the excitation and emission energies between the states with holes in the $3d_{3/2}$ and $4f_{5/2}$ core orbitals and occupation in the $5f_{5/2}$ valence orbitals. When including the SOC, the states are a linear combination of the spin-free states, and we can only obtain information about the hole and occupied valence orbital in this state from the spin-free states with the largest weights in the state with the SOC (for an overview concerning the application for heavy-metal complexes, see ref 74).

3.1. M₄ HR-XANES ($3d_{3/2} \rightarrow 5f_{5/2}$ U M₄ Absorption Edge). The three pronounced peaks in the HR-XANES (see Figure 4) are associated with an excitation from 3d $\sigma/\pi/\delta$
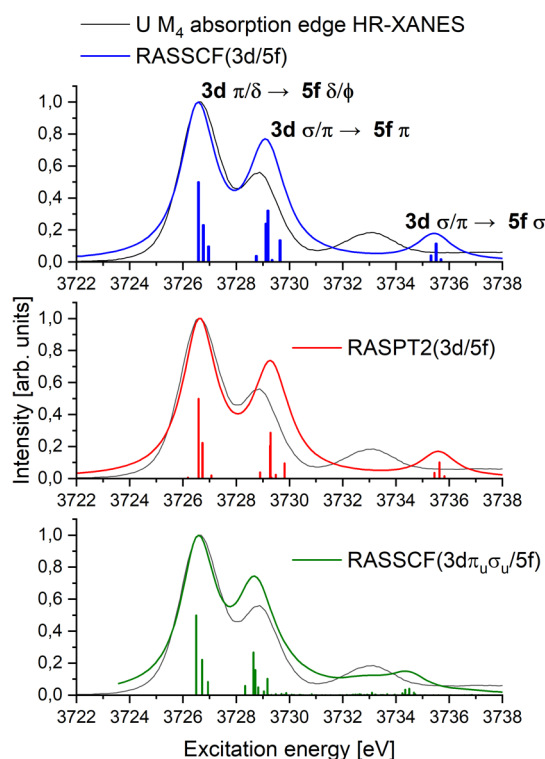
Figure 4. HR-XANES ($3d_{3/2} \rightarrow 5f_{5/2}$ U M₄ absorption edge): comparison of experimental data (black line) and calculated spectra (colored lines) obtained with different methods or active spaces. The calculated spectra are shown together with the transition energies and the corresponding oscillator strengths. The oscillator strengths are scaled to fit to the experimental data (colored bars) (energies in eV).

orbitals into the 5f δ/ϕ, 5f π^*, and 5f σ^* orbitals (see Figures 1 and 3a). These peaks are well-resolved and assigned both experimentally[2,8] and in simulations of the spectra based on *ab*

initio calculations.[3] First, we compare the simulated U M₄ absorption edge spectra with the experimental data. The simulated spectra based on the calculated transition energies and oscillator strengths and the excellent agreement between the theoretical and experimental data sets show the high quality of our calculated data. Subsequently, we give a detailed assignment of the occupation of the 5f valence shell and the location of the hole in the 3d shell of UO_2^{2+} of all the calculated excited states with and without the SOC.

All the calculated positions and splittings are shown in Table 1. The experimental and calculated HR-XANES spectra are presented in Figure 4 together with the calculated transition energies and corresponding (scaled) oscillator strengths. The splitting of the energies shows the multiplet splitting in the HR-XANES spectra of uranyl. For the simulation of the spectra, we applied a Lorentzian lifetime broadening of 1.5 eV, which reproduced the experimental spectra the best.

The calculated RASSCF (3d/5f) HR-XANES spectrum with the minimal active space was shifted by −24.0 eV and the RASPT2 (3d/5f) HR-XANES spectrum by −19.5 eV to align the main peak of the simulation with the experimental data. The RASSCF (3d $\sigma_u\pi_u$/5f) result shows a much better agreement with the experiment than the RASSCF (3d/5f) calculations and was shifted by −21.4 eV. The applied shifts for our results agree very well with the shift reported by Sergentu et al. (−23.5 eV)[3] for uranyl. The origin of this shift is the systematic error in the *ab initio* calculations. They are different for the calculation of the excitation and below for the RIXS calculations and also for the emission energies. The magnitude of 10−25 eV is to be expected and is rather small compared to the absolute value of the transition energies.

The calculated splittings between the three peaks are slightly better described by the RASSCF (3d/5f) calculations (+2.5/+8.8 eV) compared to that by RASPT2 (3d/5f) (+2.7/+9.0 eV). Both splittings with the minimal (3d/5f) active space are consistently too large. A considerable improvement (see Table 1) of the calculated splittings can be observed upon enlarging the active space by the three occupied σ_u/π_u orbitals. The RASSCF (3d $\sigma_u\pi_u$/5f) splittings (+2.1/+7.7 eV) agree very well with the experimental findings (+2.2/+6.7 eV) and the *ab initio* results of Sergentu et al.[3] (+2.3/+7.9 eV). Thus, the inclusion of the bonding σ_u and two π_u orbitals in the RAS2 active space decreases the required shift to align with the experimental data and the splitting between the peaks, but the increase in the computational cost to achieve this is huge.

All the relevant excited states $|(3d_{3/2})^{-1}(5f_{5/2})^1\rangle$ involved in the U M₄ absorption edge spectra have a hole in the $3d_{3/2}$ shell and one electron in an $5f_{5/2}$ valence orbital. The calculated splitting of the U $M_{4,5}$ edges ($3d_{5/2} \rightarrow 5f_{5/2,7/2}$ U M₅ absorption edge) of 173 eV fits very well to the observed value of 176 eV.

Table 1. Calculated and Experimental Peak Positions of the HR-XANES ($3d_{3/2} \rightarrow 5f_{5/2}$ U M₄ Absorption Edge) (Energies in eV)

method	active space	basis set	references	peak position $E(5f \delta/\phi)$	peak splitting $\Delta E = E(5f \sigma^*/5f \pi^*) - E(5f \delta/\phi)$	
					5f π^*	5f σ^*
experiment			2	3726.6	+2.2	+6.7
RASSCF		ANO-VTZ	3	3750.1	+2.3	+7.9
RASSCF	3d/5f	ANO-VQZ	this work	3750.6	+2.5	+8.8
RASPT2	3d/5f	ANO-VQZ	this work	3746.1	+2.7	+9.0
RASSCF	3d $\sigma_u\pi_u$/5f	ANO-VQZ	this work	3748.0	+2.1	+7.7
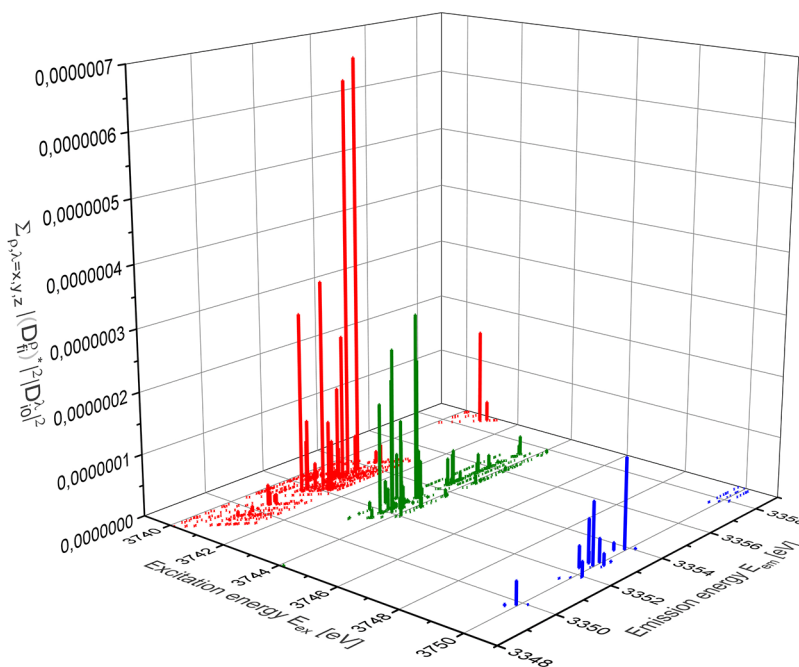
Figure 5. $\sum_{\rho,\lambda=x,y,z}|\langle f|\hat{\mu}_\rho|i\rangle|^2|\langle i|\hat{\mu}_\lambda|0\rangle|^2$ at the corresponding resonant excitation $E_{ex} = E_i - E_0$ and emission $E_{em} = E_i - E_f$ energies of the 3d4f RIXS map (all energies in eV). The red bars show $\sum_{\rho,\lambda=x,y,z}|\langle f|\hat{\mu}_\rho|i\rangle|^2|\langle i|\hat{\mu}_\lambda|0\rangle|^2$ with the intermediate states $i \in$ 5f δ, 5f ϕ, the green bars with $i \in$ 5f π^*, and the blue bars with $i \in$ 5f σ^*.

The ground state of UO_2^{2+} is closed-shell. Hence, the excited states including SOC with allowed transition dipole moments from the ground state are only a few. Therefore, there are only a few electronic transitions shaping the form of the U M_4 absorption edge spectra. The SOC calculation is based on the ground state and 35 excited spin-free states in A_u symmetry with singlet and triplet spins, each. In the final SOC calculation, we include 140 excited states.

The relevant excited electronic states for the first peak at 3726.6 eV can be assigned to SOC states which are a linear combination of the singlet and triplet (spin-free) states, and their weights are 0.33 and 0.27, respectively. Both states are in turn a linear combination of several configurations such as $|(3d \delta)^{-1}(5f \phi)^1\rangle$, $|(3d \pi)^{-1}(5f \delta)^1\rangle$, and $|(3d \sigma)^{-1}(5f \pi)^1\rangle$. In total, the weight of the configurations in the relevant SOC states with $|(3d \delta)^{-1}(5f \phi)^1\rangle$ is 0.34, with $|(3d \pi)^{-1}(5f \delta)^1\rangle$ is 0.18, and with $|(3d \sigma)^{-1}(5f \pi)^1\rangle$ is 0.12 (plus many smaller contributions from other configurations). Therefore, they are mainly formed by spin-free states with an occupied 5f δ/ϕ orbital and one hole in a 3d π/δ orbital $|(3d \pi/\delta)^{-1}(5f \delta/\phi)^1\rangle$. Hence, these excited states show a pronounced multiconfigurational character, the SOC state is formed by spin-free states with nearly equal weights, and the spin-free states are, by themselves, also formed from several different configurations. For this peak at 3726.6 eV, there are also small contributions from the excitation into an $|(3d \pi/\delta)^{-1}(5f \pi/\phi)^1\rangle$ excited state.

The excited electronic states contributing to the second peak at 3728.8 eV have one electron occupying a 5f π^* orbital and one hole in a 3d σ/π orbital $|(3d \sigma/\pi)^{-1}(5f \pi^*)^1\rangle$. The excited states with the highest excitation energy at 3233.3 eV are formed by states with one electron occupying a 5f σ^* orbital and one hole in a 3d σ/π orbital $|(3d \sigma/\pi)^{-1}(5f \sigma^*)^1\rangle$.[b] Hence, our assignment is in total agreement with former results.[2,3,8] The shape of the spectra is determined by the splitting of the 5f σ^*, 5f π^*, 5f δ, and 5f ϕ orbitals in the presence of the two oxygen ions in UO_2^{2+}. The splitting of the five 3d orbitals ($\Delta E_{3d} \approx 0.3$ eV) has hardly an influence on the U M_4 absorption edge spectra. The splitting is so small because they are core electrons (we determined this splitting by calculating the electronic energies of the UO_2^{3+} states with one hole in the 3d shell).

From the calculations, we can show that the atomic spin orbitals of uranium correspond in good approximation to spin-free MOs of uranyl, $5f_{5/2}(m_J = 5/2) \approx$ 5f ϕ orbitals and correspondingly $5f_{5/2}(m_J = 3/2) \approx$ 5f δ and $5f_{5/2}(m_J = 1/2) \approx$ 5f π^*/σ^*. For the $3d_{3/2}$ orbitals, we find $3d_{3/2}(m_J = 3/2) \approx$ 3d δ orbitals and $3d_{3/2}(m_J = 1/2) \approx$ 3d π/σ.

The active space for an accurate calculation on uranyl should include all bonding and antibonding orbitals of uranyl[66,67] (see Figure 1). In our calculation, this would lead to a prohibitively large active space. Therefore, the main source of the large error of the excitation energies into the 5f σ^* orbitals and the splitting of $\Delta E = E(5f \sigma^*) - E(5f \delta/\phi) = 8.8$ eV (RASSCF)/9.0 eV (RASPT2) (see Table 1) is the choice of the small active space. Increasing the active space leads to a reduction of the splitting to $\Delta E = E(5f \sigma^*) - E(5f \delta/\phi) = 7.7$ eV. This is in much better agreement with the experimental results and the result reported by Sergentu et al.[3] The inclusion of the dynamic correlation does not improve the result at all. However, with the minimal active space, we are able to reproduce the experimental HR-XANES spectra such that a clear and unambiguous theoretical assignment of all observed features in the HR-XANES spectra can be carried out.

3.2. 3d4f RIXS Map (U M_4 Absorption Edge and $4f_{5/2} \rightarrow 3d_{3/2}$ U M_β Emission). The 3d4f RIXS map is fully characterized by calculating all excitation energies between the ground $|0\rangle$ and intermediate states $|(3d_{3/2})^{-1}(5f_{5/2})^1\rangle$ of the U M_4 absorption and emission energies between the intermediate and final states $|(4f_{5/2})^{-1}(5f_{5/2})^1\rangle$ of the U M_β emission together with the corresponding transition dipole moments.

The numerator of the Kramers−Heisenberg formula $\sum_{\rho,\lambda=x,y,z}|\langle f|\hat{\mu}_\rho|i\rangle|^2|\langle i|\hat{\mu}_\lambda|0\rangle|^2$ (see eq 4) is a measure of the signal strength at the resonant excitation $E_{ex} = E_i - E_0$ and emission E_{em}
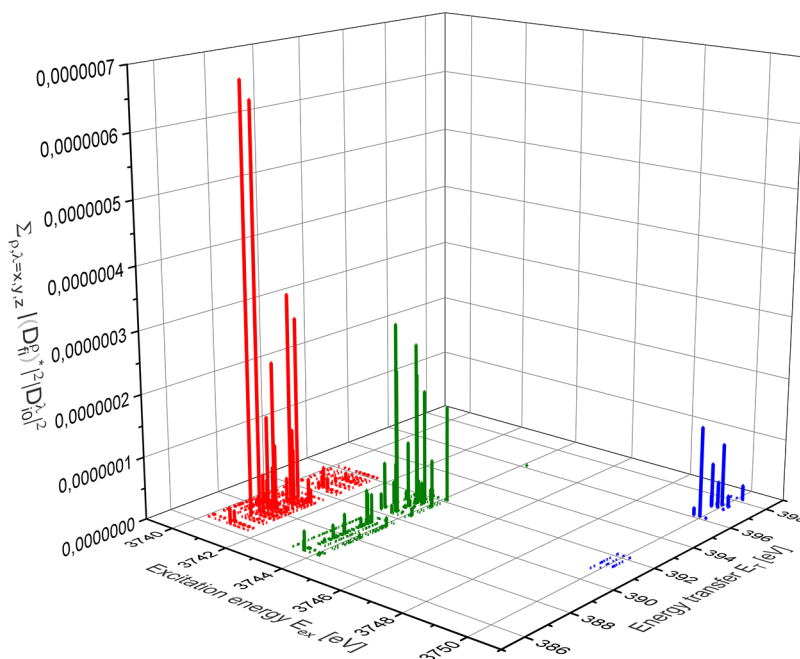
Figure 6. $\sum_{\rho,\lambda=x,y,z} |\langle f|\hat{\mu}_\rho|i\rangle|^2 |\langle i|\hat{\mu}_\lambda|0\rangle|^2$ at the corresponding resonant excitation $E_{ex} = E_i - E_0$ and energy transfer $E_T = E_{ex} - E_{em} = E_f - E_0$ of the 3d4f RIXS map (all energies are in eV, and the color scheme is the same as that in Figure 5).

$= E_i - E_f$ energies (or energy transfer $E_T = E_f - E_0$) of the RIXS map (see eqs 3, 4 and 9−11 in ref 24). They are shown in Figure 5 as vertical bars for the most intense transitions contributing to the 3d4f RIXS map of uranyl. The graphical representation of the data in Figure 5 allows an intuitive and transparent understanding of the calculated 3d4f RIXS map. The vertical bars colored in red belong to RIXS processes involving 5f δ or 5f ϕ unoccupied valence orbitals, vertical bars in green involve 5f π^*, and blue-colored bars involve 5f σ^* orbitals. With this in mind, the 3d4f RIXS map can be assigned straightforwardly. Figure 5 shows also that the 3d4f RIXS map consists of many different excitation/emission processes which contribute to the different pronounced peaks. The corresponding results for the numerator depending on E_{ex}/E_T are shown in Figure 6.

The calculated 3d4f RIXS map in Figure 7a was determined based on eqs 1 and 2. In eq 1, the complex contributions from all of the intermediate states of the RIXS process are summed up in the numerator before squaring, fully including the interference effects. The calculated 3d4f RIXS map agrees very well with the experimental data shown in Figure 7d.[2] The peak positions are shown in Table 2 and compared with those obtained in the experiment. We applied the Lorentzian lifetime broadenings Γ_i = 3.0 eV and Γ_f = 0.15 eV. These broadenings compare very well to the data reported by others[2,75,76] (Γ_i = 3.2 eV and Γ_f = 0.28 eV).

We analyze the features of the RIXS map step-by-step. The main feature is the three pronounced peaks of the RIXS map. Their excitation energies are well-separated, and their emission energies are slightly red-shifted when moving from lower to higher excitation energies.

The peak position of the most intense peak corresponding to excitations involving the 5f δ/ϕ orbitals is shifted by ΔE_{ex} = −13.6 eV for the excitation energy and ΔE_{em} = −21.2 eV for the emission energy to align with the experimental data. The corresponding results depending on E_{ex}/E_T are shown in Figure 8. The 3d4f RIXS map depending on the excitation energy E_{ex} and the energy transfer $E_T = E_{ex} - E_{em}$ is shown in Figure 8a. The

peak position of the most intense peak has a shift of ΔE_T = −7.6 eV to align with the experimental results.

Most pronounced is the feature corresponding to the transitions into the 5f δ/ϕ, 5f π^*, and 5f σ^* orbitals (see Figures 1 and 3a) and the observed splittings between the three peaks regarding the relevant excitation and emission energies. The calculated splittings $\Delta E_{ex}(5f\,\pi^* - 5f\,\delta/\phi)$ = +2.5 eV and $\Delta E_{ex}(5f\,\sigma^* - 5f\,\delta/\phi)$ = +9.0 eV are too large compared with the experimental values $\Delta E_{ex}(5f\,\pi^* - 5f\,\delta/\phi)$ = +1.7 eV and $\Delta E_{ex}(5f\,\sigma^* - 5f\,\delta/\phi)$ = +6.0 eV due to the small (3d/5f) active space, as discussed above (see Section 4.1). The splittings of the emission energies are reproduced very well by the calculations, $\Delta E_{em}(5f\,\pi^* - 5f\,\delta/\phi)$ = −0.6 eV and $\Delta E_{em}(5f\,\sigma^* - 5f\,\delta/\phi)$ = −0.7 eV, compared with the experimental values of $\Delta E_{em}(5f\,\pi^* - 5f\,\delta/\phi)$ = −0.6 eV and $\Delta E_{em}(5f\,\sigma^* - 5f\,\delta/\phi)$ = −0.5 eV.

In contrast to the 3d orbitals, which have a very small splitting due to the presence of the oxygen ions, the situation is different for the emission energies when the 4f orbitals are involved since they are much closer to the valence orbitals (see Figures 1 and 3b). A separate calculation of the energies of the electronic energies of the UO_2^{3+} states with one hole in the 4f shell shows that $\Delta E_{4f} \approx 0.9$ eV, comparable to the red shift of 5f π^* and 5f σ^* with respect to the 5f δ/ϕ peak observed in the RIXS map.[2] In the previous section, Section 4.1, we identified the occupied states in the 5f orbitals and the holes in the 3d orbitals upon $3d_{3/2} \rightarrow 5f_{5/2}$ excitations. The holes are filled by electrons from the $4f_{5/2}$ orbitals. The selection rules for $3d_{3/2} \rightarrow 5f_{5/2}$ and $4f_{5/2} \rightarrow 3d_{3/2}$ are identical. Thus, upon emission, the 3d holes can be filled by electrons from the $4f_{5/2}$ orbitals with the same m_J as occupied in the $5f_{5/2}$ shell. However, there are also a few other possible $4f_{5/2} \rightarrow 3d_{3/2}$ transitions. Therefore, the exact calculations of the dipole transition matrix element provide this important information.

As mentioned earlier in the assignment of the involved spin-free MOs (3d and 5f) in the HR-XANES section, there is a correspondence between the atomic 4f spin orbitals and the spin-free MOs of uranyl: $4f_{5/2}(m_J = 5/2) \approx 4f\,\phi$ orbitals and
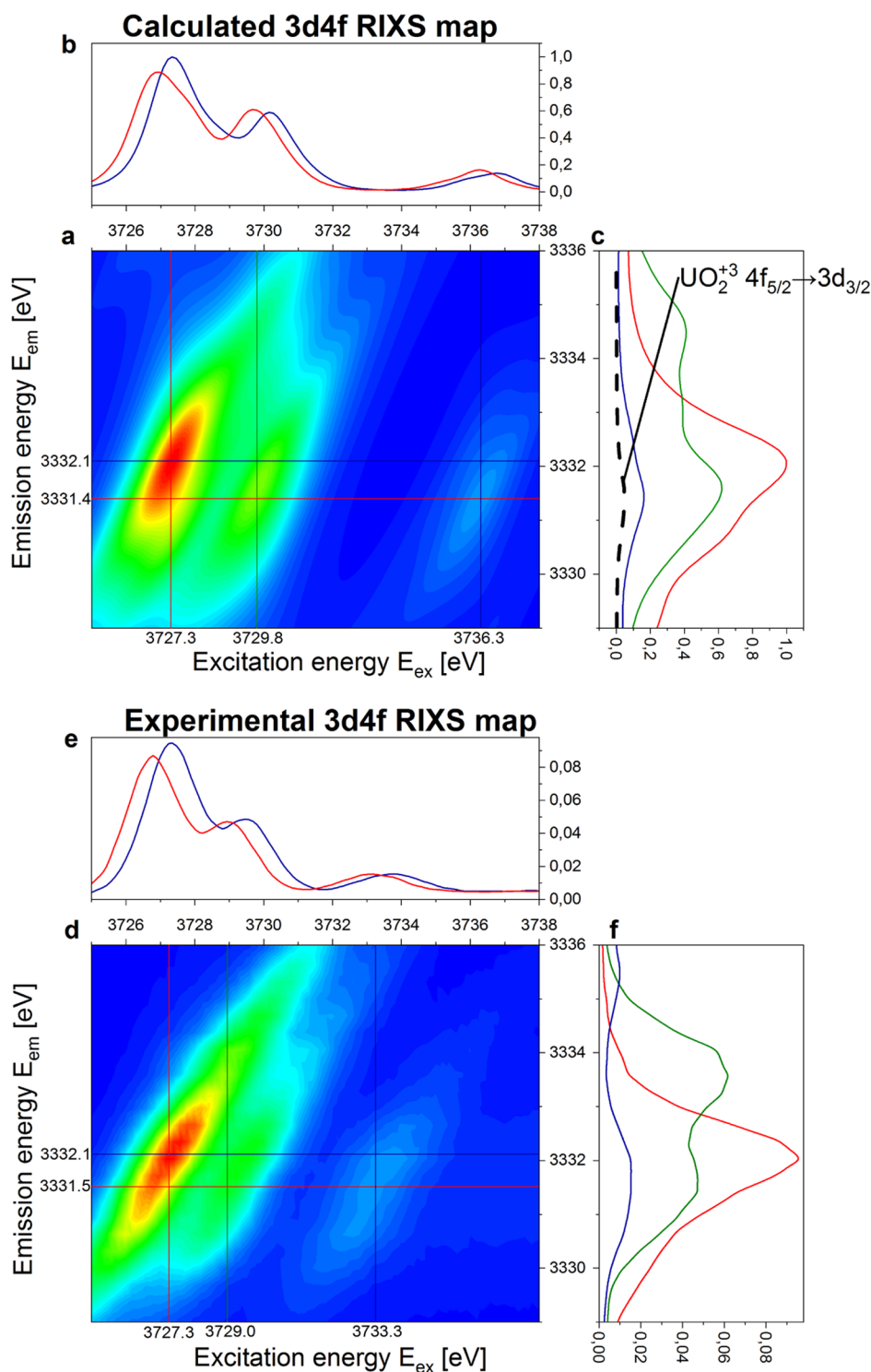
Figure 7. RASPT2 calculated and experimental[2] (see Figure 3a therein) 3d4f RIXS maps of uranyl UO_2^{2+} depending on the excitation energy E_{ex} and emission energy E_{em}. (a) Calculated and shifted ($\Delta E_{ex} = -13.6$ eV/$\Delta E_{em} = -21.2$ eV) 3d4f RIXS map. (b) Calculated HR-XANES spectra at the maximum of the resonant (3332.1 eV) and non-resonant (normal) emission (3331.4 eV). (c) RIXS emission lines calculated at the three peak maxima and calculated $4f_{5/2} \rightarrow 3d_{3/2}$ transitions of UO_2^{3+} (dashed black line). (d) Experimental 3d4f RIXS map. (e) HR-XANES spectra measured at the maximum of the resonant (3332.1 eV) and nonresonant (normal) emission (3331.5 eV). (f) RIXS emission lines measured at the three peak maxima (all energies are in eV).

correspondingly $4f_{5/2}(m_J = 3/2) \approx 4f\,\delta$ and $4f_{5/2}(m_J = 1/2) \approx 4f\,\pi/\sigma$.

The calculations show that for the first peak at 3727.3 eV, the most intense emissions following the excitation 3d $\pi/\delta \rightarrow$ 5f δ/ϕ is a 4f $\delta/\phi \rightarrow$ 3d π/δ emission, leaving 5f δ/ϕ occupied and a

hole in $4f\,\delta/\phi$ ($|(3d\,\pi/\delta)^{-1}(5f\,\delta/\phi)^1\rangle \rightarrow |(4f\,\delta/\phi)^{-1}(5f\,\delta/\phi)^1\rangle$) (see Table 3). Accordingly we found for the two other peaks the $|(4f\,\pi)^{-1}(5f\,\pi^*)^1\rangle$ and $|(4f\,\sigma)^{-1}(5f\,\sigma^*)^1\rangle$ states as final states. Hence, the occupied 5f valence and 4f core hole orbitals have the same m_J. For all the assigned holes in the 4f shell, we determined

Table 2. Peak Positions of the 3d4f RIXS Map of Uranyl and Positions of the Maxima of the Resonant and Non-resonant (Normal) Emission (See Figure 3 in ref 2)[a]

	excitation energy E_{ex}		emission energy E_{em}		energy transfer $E_T = E_{ex} - E_{em}$	
		Theory: RASPT2 Calculations				
5f δ/ϕ	3727.3		3332.1		395.2	
5f $\pi*$	3729.8	+2.5	3331.5	−0.6	398.3	+3.1
5f $\sigma*$	3736.3	+9.0	3331.4	−0.7	404.9	+9.7
resonant emission			3332.1			
non-resonant (normal) emission			3331.4			
		Experiment[2]				
5f δ/ϕ	3727.3		3332.1		395.2	
5f $\pi*$	3729.0	+1.7	3331.5	−0.6	397.5	+2.3
5f $\sigma*$	3733.3	+6.0	3331.6	−0.5	401.7	+6.5
resonant emission			3332.1			
non-resonant (normal) emission			3331.5			

[a]All the calculated values are shifted by $\Delta E_{ex} = -13.6$ eV, $\Delta E_{em} = -21.2$ eV, and $\Delta E_T = \Delta E_{ex} - \Delta E_{em} = +7.6$ eV to align with the experimental data (energies in eV).

the orbitals from the spin-free states with the highest weight in the states including SOC. From Figures 5 and 6, we see that there are always smaller contributions of other transitions to states with holes in other 4f orbitals. We find the largest contribution of transitions to other states for the peak at 3727.3 eV with a final state of $|(4f\ \pi)^{-1}(5f\ \delta)^1\rangle$ and for the second peak at 3729.8 eV with the final state of $|(4f\ \sigma)^{-1}(5f\ \pi*)^1\rangle$.

Since the 4f σ/π orbitals are higher in energy compared to the 4f δ/ϕ orbitals, creating a hole in 4f δ/ϕ releases more energy and $\Delta E_{4f\delta/\phi \to 3d\delta} > \Delta E_{4f\sigma/\pi \to 3d\sigma/\pi}$. Therefore, the splitting between these three peaks, which is observed in emission, corresponds in good approximation (since the splitting of the 3d states is small) to the fine structure splitting of the 4f states in the presence of the two oxygen ions (see Figure 3). From Table 2, we see that the $\Delta E_{4f\delta/\phi - 4f\pi}$ splitting is 0.6 eV and the $\Delta E_{4f\delta/\phi - 4f\sigma}$ splitting is 0.7 eV. This is comparable to the splitting of the RASSCF/RASPT2 4f orbitals in the uranyl ground state. In the energy transfer picture (see Figure 8 and Table 2), the influence of the position of the hole in the 3d shell is completely removed, and we get direct information about the $\Delta E_{5f\delta/\phi - 4f\delta/\phi} = 395.2$ eV, $\Delta E_{5f\pi* - 4f\pi} = 398.3$ eV, and $\Delta E_{5f\sigma* - 4f\sigma} = 404.9$ eV splittings. All the calculated values agree very well with the measured data.

The maximum of the resonant emission of the RIXS map is the maximum of the emission, attributed to the 5f δ/ϕ peak at 3332.1 eV. The maximum of the non-resonant (normal) emission was determined in a separate calculation ($3d^9 4f^{14} \to 3d^{10} 4f^{13}$ transitions of UO_2^{3+}, see Table 2 and Figure 7c) to be 3331.4 eV. The calculated ($\Delta E_{res/non-res} = 0.7$ eV) and experimental values ($\Delta E_{res/non-res} = 0.6$ eV) of this shift agree with high accuracy. The position of the two maxima are indicated as horizontal lines in Figure 7a,d. This result is an additional point verifying the high quality of our calculations.

Vitova et al.[2] (see Figure 3d therein) found U M_4 absorption edge HR-XANES spectra of UO_2^{2+} determined at the maxima of the resonant and non-resonant (normal) emission to be very similar for uranyl. We determined the HR-XANES spectra extracted at these two positions and found excellent agreement with the experimental data (see Figure 7b,e and Table 4). The high similarity of the two HR-XANES spectra extracted at the two emission maxima is solely due to the small red shift between the emission energies of the three dominant peaks in the 3d4f RIXS map, and this in turn is caused by the small splitting of the $4f_{5/2} \to 3d_{3/2}$ U M_β emission in UO_2^{2+}.

4. CONCLUSIONS

This excellent agreement between our theoretical data and the measurements shows that the approach using the RASSCF/RASPT2 methods followed by the inclusion of SOC is applicable to the accurate calculation of An $M_{4,5}$ HR-XANES (in agreement with Sergentu et al.[3]) and 3d4f RIXS maps and reproduces the multiplet structure of the uranyl spectra faithfully. We show that the multiconfigurational protocol, which is nowadays applied as a standard tool to study the X-ray spectra of transition metal complexes, can be extended to the calculations of RIXS maps of An compounds. They have many intermediate- and final-state multiplets of the RIXS process with rather complicated electronic structures, and they can be accurately described with our theoretical approach.

The high quality of the calculated data allows for the clarification of the considered open questions concerning the features observed in the experimental 3d4f RIXS map[2]

(1) all intermediate and final states responsible for the different features of the 3d4f RIXS map could be completely assigned;

(2) the three distinct peaks in the RIXS map display the splitting of the 5f (in excitation) and 4f orbitals (in emission). The calculations show that in emission, the fine structure of the 4f orbitals is resolved and that in the energy transfer picture, the ΔE_{4f-5f} excitation energies can be accurately determined;

(3) the calculated positions of the maxima of the resonant (UO_2^{2+}) and non-resonant (normal, UO_2^{3+}) emissions agree very well with the experimental data; and

(4) the simulated HR-XANES spectra at these two different energies reproduce the experimental result very accurately.

These results allow for a deeper understanding of the experimental 3d4f RIXS map of uranyl with the help of our relativistic multiconfigurational *ab initio* calculations.

The calculation of RIXS maps involving An species with relativistic multiconfigurational *ab initio* methods complements the experimental efforts in this field greatly and allows for the interpretation of the 3d4f RIXS map of uranyl in a clear and transparent way. The calculations presented in this work establish relativistic multiconfigurational *ab initio* calculations as a new powerful tool for the calculation of RIXS maps involving An.
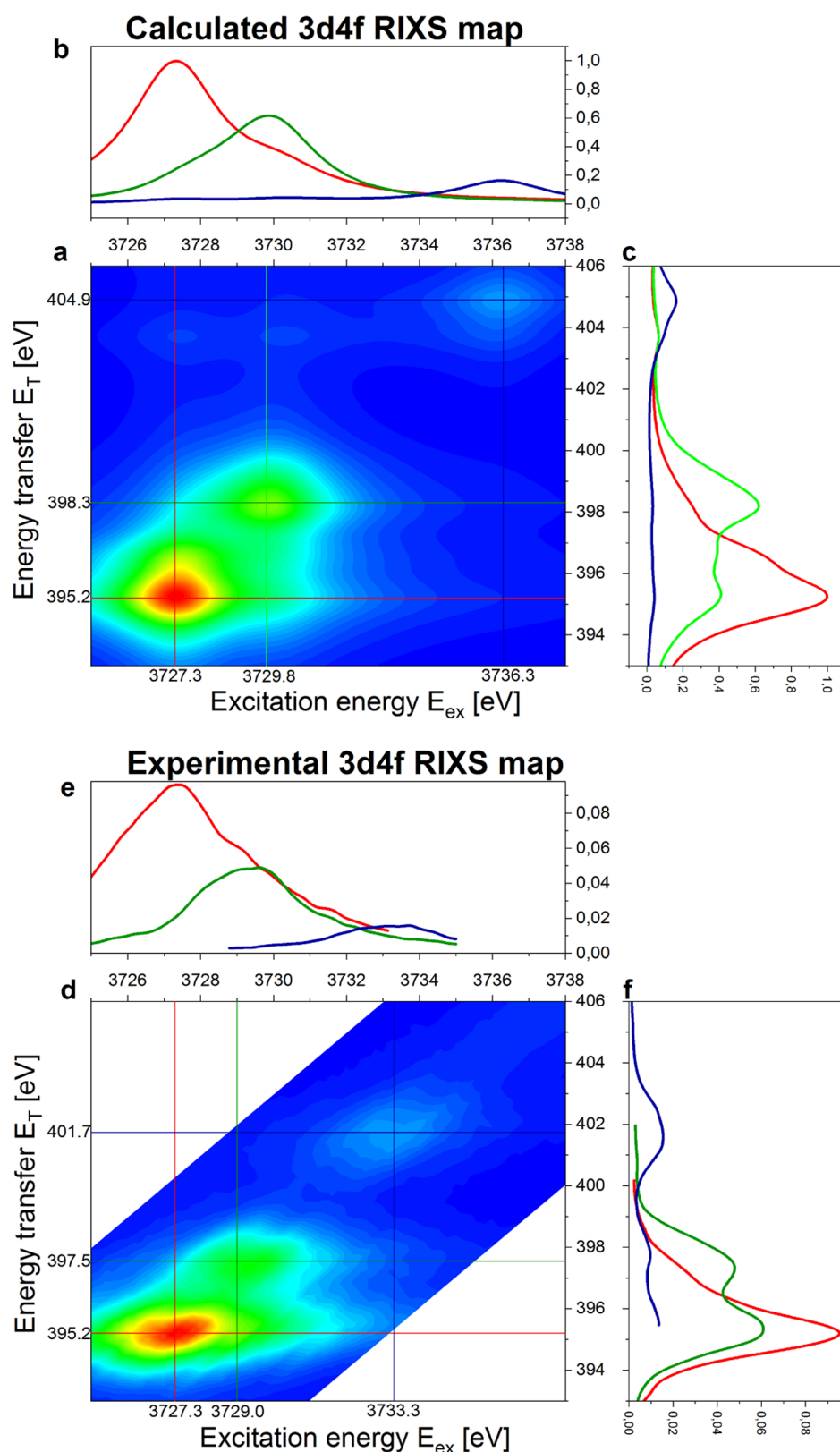
Figure 8. RASPT2 calculated and experimental[2] 3d4f RIXS maps of uranyl UO_2^{2+} depending on the excitation energy E_{ex} and energy transfer E_T. (a) Calculated and shifted ($\Delta E_{ex} = -13.6$ eV/$\Delta E_i = +7.6$ eV) 3d4f RIXS map. (b) Calculated contour profiles of the excitation energies at the maximum emission energies of the three peaks. (c) Calculated contour profile of the emission energies at the maximum excitation energies of the three peaks. (d) Experimental 3d4f RIXS map. (e) Measured contour profile of the excitation energies at the maximum emission energies of the three peaks. (f) Measured contour profile of the emission energies at the maximum excitation energies of the three peaks (all energies are in eV).

Table 3. Intermediate and Final States of the Three Most Pronounced Peaks in the 3d4f RIXS Map (Energies in eV)

peak position					
excitation energy	emission energy	excitation	intermediate state	emission	final state
3727.3	3332.1	$3d\pi/\delta \rightarrow 5f\, \delta/\phi$	$|(3d\,\pi/\delta)^{-1}(5f\,\delta/\phi)^1\rangle$	$4f\,\delta/\phi \rightarrow 3d\,\pi/\delta$	$|(4f\,\delta/\phi)^{-1}(5f\,\delta/\phi)^1\rangle$
3729.8	3331.5	$3d\,\sigma/\pi \rightarrow 5f\,\pi^*$	$|(3d\,\sigma/\pi)^{-1}(5f\,\pi^*)^1\rangle$	$4f\,\pi \rightarrow 3d\,\sigma/\pi$	$|(4f\,\pi)^{-1}(5f\,\pi^*)^1\langle$
3736.3	3331.4	$3d\,\sigma/\pi \rightarrow 5f\,\sigma^*$	$|(3d\,\sigma/\pi)^{-1}(5f\,\sigma^*)^1\langle$	$4f\,\sigma \rightarrow 3d\,\sigma/\pi$	$|(4f\,\sigma)^{-1}(5f\,\sigma^*)^1\langle$

Table 4. Comparison of the Calculated Peak Positions of the HR-XANES Spectra along the Maxima of the Resonant and Non-resonant Emission (See Table 2), as Indicated in Figure 7, and the Experimental Data of Vitova et al.[2] (See Figure 3d therein)[a]

	$E\,(5f\,\delta/\phi)$	$\Delta E = E(5f\,\pi^*) - E(5f\,\delta/\phi)$	$\Delta E = E(5f\,\sigma^*) - E(5f\,\delta/\phi)$
	Theory: RASPT2 Calculations		
resonant emission at 3332.1	3727.3	+2.9	+9.5
non-resonant (normal) emission at 3331.4	3726.9	+2.8	+9.4
	Experiment[2]		
resonant emission at 3332.1	3727.3	+2.3	+6.4
non-resonant (normal) emission at 3331.5	3726.7	+2.1	+6.5

[a]All the calculated values are shifted by $\Delta E_{ex} = -13.6$ eV to align with the experimental data (energies in eV).

■ AUTHOR INFORMATION

Corresponding Author

Robert Polly − *Karlsruher Institut für Technologie (KIT), Institut für Nukleare Entsorgung (INE), 76021 Karlsruhe, Germany;* ⓞ orcid.org/0000-0002-7024-7987;
Email: polly@kit.edu

Authors

Bianca Schacherl − *Karlsruher Institut für Technologie (KIT), Institut für Nukleare Entsorgung (INE), 76021 Karlsruhe, Germany;* ⓞ orcid.org/0000-0003-4542-0108

Jörg Rothe − *Karlsruher Institut für Technologie (KIT), Institut für Nukleare Entsorgung (INE), 76021 Karlsruhe, Germany;*
ⓞ orcid.org/0000-0001-5366-2129

Tonya Vitova − *Karlsruher Institut für Technologie (KIT), Institut für Nukleare Entsorgung (INE), 76021 Karlsruhe, Germany;* ⓞ orcid.org/0000-0002-3117-7701

Complete contact information is available at:
https://pubs.acs.org/10.1021/acs.inorgchem.1c02364

Notes

The authors declare no competing financial interest.

■ ADDITIONAL NOTES

[a]Alternatively, using the MOs, the active space can be formed by $2 \times \pi_u$, $2 \times \pi_g$, σ_u, σ_g, $2 \times \delta_u$, $2 \times \phi_u$, $2 \times \pi_u^*$, σ_u, $2 \times \pi_g^*$, and σ_g^* (see Figure 1).

[b]The final states of the M_4 HR-XANES are the intermediate states of the 3d4f RIXS process (see also Table 3).

■ REFERENCES

(1) Morss, L. R.; Edelstein, N. M.; Fuger, J. *The Chemistry of the Actinide and Transactinide Elements*; Springer: Dordrecht, 2006.

(2) Vitova, T.; Pidchenko, I.; Fellhauer, D.; Bagus, P.; Joly, Y.; Prüssmann, T.; Bahl, S.; Gonzalez-Robles, E.; Rothe, J.; Altmaier, M.; Denecke, M.; Geckeis, H. The role of the 5f valence orbitals of early actinides in chemical bonding. *Nat. Commun.* 2017, 8, 1−9.

(3) Sergentu, D.-C.; Duignan, T. J.; Autschbach, J. Ab Initio Study of Covalency in the Ground versus Core-Excited States and X-ray Absorption Spectra of Actinide Complexes. *J. Phys. Chem. Lett.* 2018, 9, 5583.

(4) Bagus, P.; Schacherl, B.; Vitova, T. Computational and spectroscopic tools for detection of bond covalency in Pu(IV) materials. *Inorg. Chem.* 2021, 60, 16090.

(5) Butorin, S. M.; Mancini, D. C.; Guo, J.-H.; Wassdahl, N.; Nordgren, J.; Nakazawa, M.; Tanaka, S.; Uozumi, T.; Kotani, A.; Ma, Y.; Myano, K. E.; Karlin, B. A.; Shuh, D. K. Resonant X-Ray Fluorescence Spectroscopy of Correlated Systems: A Probe of Charge-Transfer Excitations. *Phys. Rev. Lett.* 1996, 77, 574.

(6) Kvashnina, K. O.; Butorin, S. M.; Martin, P.; Glatzel, P. Chemical state of complex uranium oxides. *Phys. Rev. Lett.* 2013, 111, 253002.

(7) Vitova, T.; Denecke, M. A.; Göttlicher, J.; Jorissen, K.; Kas, J. J.; Kvashnina, K.; Prüßmann, T.; Rehr, J. J.; Rothe, J. Actinide and lanthanide speciation with high-energy resolution X-ray techniques. *J. Phys.* 2013, 430, 012117.

(8) Vitova, T.; Green, J. C.; Denning, R. G.; Löble, M.; Kvashnina, K.; Kas, J. J.; Jorissen, K.; Rehr, J. J.; Malcherek, T.; Denecke, M. A. Polarization Dependent High Energy Resolution X-ray Absorption Study of Dicesium Uranyl Tetrachloride. *Inorg. Chem.* 2015, 54, 174.

(9) Butorin, S. M.; Kvashnina, K. O.; Vegelius, J. R.; Meyer, D.; Shuh, D. K. High-resolution X-ray absorption spectroscopy as a probe of crystal-field and covalency effects in actinide compounds. *Proc. Natl. Acad. Sci. U. S. A.* 2016, 113, 8093.

(10) Podkovyrina, Y.; Pidchenko, I.; Prüßmann, T.; Bahl, S.; Göttlicher, J.; Soldatov, A.; Vitova, T. Probing covalency in UO3 polymorphs by U M4 edge HR-XANES. *J. Phys.: Conf. Ser.* 2016, 712, 012092.

(11) Schülke, W. *Electron Dynamics by Inelastic X-Ray Scattering*; Oxford Series on Synchrotron Radiation: Oxford, 2007.

(12) Ament, L. J. P.; van Veenendaal, M.; Devereaux, T. P.; Hill, J. P.; van den Brink, J. Resonant Inelastic X-Ray Scattering Studies of Elementary Excitations. *Rev. Mod. Phys.* 2011, 83, 705.

(13) Gel'mukhanov, F.; Ågren, H. Resonant X-ray Raman scattering. *Phys. Rep.* 1999, 312, 87.

(14) Carra, P.; Fabrizio, M.; Thole, B. T. High-resolution X-ray resonant raman-scattering. *Phys. Rev. Lett.* **1995**, *74*, 3700.

(15) Nitsche, H. Introduction to Nuclear Chemistry. *Chem. Rev.* **2013**, *113*, 855.

(16) Geckeis, H.; Lützenkirchen, J.; Polly, R.; Rabung, T.; Schmidt, M. Mineral-Water Interface Reactions of Actinides. *Chem. Rev.* **2013**, *113*, 1016.

(17) Altmaier, M.; Gaona, X.; Fanghänel, T. Recent Advances in Aqueous Actinide Chemistry and Thermodynamics. *Chem. Rev.* **2013**, *113*, 901.

(18) Panak, P. J.; Geist, A. Complexation and Extraction of Trivalent Actinides and Lanthanides by Triazinylpyridine N-Donor Ligands. *Chem. Rev.* **2013**, *113*, 1199.

(19) Müller, K.; et al. Interdisciplinary Round-Robin Test on Molecular Spectroscopy of the U(VI) Acetate System. *ACS Omega* **2019**, *4*, 8167.

(20) Dardenne, K.; Duckworth, S.; Gaona, X.; Polly, R.; Schimmelpfennig, B.; Pruessmann, T.; Rothe, J.; Altmaier, M.; Geckeis, H. A Combined Study of Tc Redox Speciation in Complex Aqueous Systems: Wet-Chemistry, Tc K-/L₃-Edge X-ray Absorption Fine Structure, an Ab Initio Calculations. *Inorg. Chem.* **2021**, *60*, 12285.

(21) Kramers, H. A.; Heisenberg, W. Über die Streuung von Strahlung durch Atome. *Zeitschrift fuer Physik* **1925**, *31*, 681.

(22) Sakurei, J. J. *Advanced Quantum Mechanics*; Addison-Wesley Publishing Company: Reading, 1967.

(23) Mukamel, S. Fluorescence, Spontaneus-Raman, and Coherent-Raman Spectroscopy. *Principles of Nonlinear Optical Spectroscopy*; Oxford University Press, 1999; Chapter 9.

(24) Maganas, D.; DeBeer, S.; Neese, F. A Restricted Open Configuration Interaction with Singles Method To Calculate Valence-to-Core Resonant X-ray Emission Spectra: A Case Study. *Inorg. Chem.* **2017**, *56*, 11819.

(25) Norman, P.; Dreuw, A. Simulating X-ray Spectroscopies and Calculating Core-Excited States of Molecules. *Chem. Rev.* **2018**, *118*, 7208.

(26) Lundberg, M.; Delcey, M. G. Chapter Multiconfigurational Approach to X-ray Spectroscopy of Transition Metal Complexes In *Transition Metals in Coordination Environments*; Broclawik, E., Borowski, T., Radon, M., Eds.; Springer: Cham, Switzerland, 2019.

(27) Lundberg, M.; Wernet, P. Chapter Resonant Inelastic X-ray Scattering (RIXS) Studies in Chemistry: Present and Future In *Synchrotron Light Sources and Free-Electron Lasers*; Khan, S., Schneider, J., Hastings, J., Eds.; Springer: Cham, Switzerland, 2019.

(28) Bokarev, S. I.; Kühn, O. Theoretical X-ray spectroscopy of transition metal compounds. *Wiley Interdiscip. Rev.: Comput. Mol. Sci.* **2020**, *10*, No. e1433.

(29) Pinjari, R. V.; Delcey, M. G.; Guo, M.; Odelius, M.; Lundberg, M. Restricted active space calculations of L-edge X-ray absorption spectra: From molecular orbitals to multiplet states. *J. Chem. Phys.* **2014**, *141*, 124116.

(30) Guo, M.; Källman, E.; Sørensen, L. K.; Delcey, M. G.; Pinjari, R. V.; Lundberg, M. Molecular Orbital Simulations of Metal 1s2p Resonant Inelastic X-ray Scattering. *J. Phys. Chem. A* **2016**, *120*, 5848.

(31) Kunnus, K.; Zhang, W.; Delcey, M. G.; Pinjari, R. V.; Miedema, P. S.; Schreck, S.; Quevedo, W.; Schröder, H.; Föhlisch, A.; Gaffney, K. J.; Lundberg, M.; Odelius, M.; Wernet, P. Viewing the Valence Electronic Structure of Ferric and Ferrous Hexacyanide in Solution from the Fe and Cyanide Perspectives. *Phys. Chem. B* **2016**, *120*, 7182.

(32) Josefsson, I.; Kunnus, K.; Schreck, S.; Föhlisch, A.; de Groot, F.; Wernet, P.; Odelius, M. Ab Initio Calculations of X-ray Spectra: Atomic Multiplet and Molecular Orbital Effects in a Multiconfigurational SCF Approach to the L-Edge Spectra of Transition Metal Complexes. *J. Phys. Chem. Lett.* **2012**, *3*, 3565.

(33) Atak, K.; Bokarev, S. I.; Gotz, M.; Golnak, R.; Lange, K. M.; Engel, N.; Dantz, M.; Suljoti, E.; Kühn, O.; Aziz, E. F. Nature of the Chemical Bond of Aqueous Fe²⁺ Probed by Soft X-ray Spectroscopies and ab Initio Calculations. *J. Phys. Chem. B* **2013**, *117*, 12613.

(34) Suljoti, E.; Garcia-Diez, R.; Bokarev, S. I.; Lange, K. M.; Schoch, R.; Dierker, B.; Dantz, M.; Yamamoto, K.; Engel, N.; Atak, K.; Kühn, O.; Bauer, M.; Rubensson, J.-E.; Aziz, E. F. Direct observation of molecular orbital mixing in a solvated organometallic complex. *Angew. Chem., Int. Ed.* **2013**, *52*, 9841.

(35) Bokarev, S. I.; Khan, M.; Abdel-Latif, M. K.; Xiao, J.; Hilal, R.; Aziz, S. G.; Aziz, E. F.; Kühn, O. Unraveling the Electronic Structure of Photocatalytic Manganese Complexes by L-Edge X-ray Spectroscopy. *J. Phys. Chem. C* **2015**, *119*, 19192.

(36) Wernet, P.; et al. Orbital-specific mapping of the ligand exchange dynamics of Fe(CO)₅ in solution. *Nature* **2015**, *520*, 78.

(37) Roemelt, M.; Maganas, D.; DeBeer, S.; Neese, F. A combined DFT and restricted open-shell configuration interaction method including spin-orbit coupling: Application to transition metal L-edge X-ray absorption spectroscopy. *J. Chem. Phys.* **2013**, *138*, 204101.

(38) Maganas, D.; Roemelt, M.; Hävecker, M.; Trunschke, A.; Knop-Gericke, A.; Schlögl, R.; Neese, F. First principles calculations of the structure and V L-edge X-ray absorption spectra of V2O5 using local pair natural orbital coupled cluster theory and spin−orbit coupled configuration interaction approaches. *Phys. Chem. Chem. Phys.* **2013**, *15*, 7260.

(39) Chantzis, A.; Kowalska, J. K.; Maganas, D.; DeBeer, S.; Neese, F. Ab Initio Wave Function-Based Determination of Element Specific Shifts for the Efficient Calculation of X-ray Absorption Spectra of Main Group Elements and First Row Transition Metals. *J. Chem. Theory Comput.* **2018**, *14*, 3686−3702.

(40) Maganas, D.; Kowalska, J. K.; Van Stappen, C.; DeBeer, S.; Neese, F. Mechanism of L2,3-edge x-ray magnetic circular dichroism intensity from quantum chemical calculations and experiment—A case study on V(IV)/V(III) complexes. *J. Chem. Phys.* **2020**, *152*, 114107.

(41) Maganas, D.; DeBeer, S.; Neese, F. Pair Natural Orbital Restricted Open-Shell Configuration Interaction (PNO-ROCIS) Approach for Calculating X-ray Absorption Spectra of Large Chemical Systems. *J. Phys. Chem. A* **2018**, *122*, 1215.

(42) Maganas, D.; Kristiansen, P.; Duda, L.-C.; Knop-Gericke, A.; DeBeer, S.; Schlögl, R.; Neese, F. Combined Experimental and Ab Initio Multireference Configuration Interaction Study of the Resonant Inelastic X-ray Scattering Spectrum of CO₂. *J. Phys. Chem. C* **2014**, *118*, 20163.

(43) Maganas, D.; Kowalska, J. K.; Nooijen, M.; DeBeer, S.; Neese, F. Comparison of multireference ab initio wavefunction methodologies for X-ray absorption edges: A case study on [Fe(II/III)Cl4]2−/1− molecules. *J. Chem. Phys.* **2019**, *150*, 104106.

(44) Hegarty, D.; Robb, M. A. Application of Unitary Group Methods to Configuration Interaction Calculations. *Mol. Phys.* **1979**, *38*, 1795.

(45) Roos, B. O.; Taylor, P. R.; Siegbahn, P. E. M. A complete active space SCF method (CASSCF) using a density-matrix formulated super-CI approach. *Int. J. Quant. Chem.* **1980**, *17*, 229.

(46) Siegbahn, P. E. M.; Almlöf, J.; Heiberg, A.; Roos, B. O. The complete active space SCF method (CASSCF) in a Newton-Raphson formulation with application to the HNO molecule. *J. Chem. Phys.* **1981**, *74*, 2384.

(47) Hegarty, D. Application of Unitary Group Methods to Configuration Interaction Calculations. *Adv. Chem. Phys.* **1987**, *69*, 399.

(48) Malmqvist, P. A.; Rendell, A.; Roos, B. O. The restricted active space self-consistent-field method, implementerd with a split graph unitary-group approach. *J. Phys. Chem.* **1990**, *94*, 5477.

(49) Andersson, K.; Malmqvist, P. A.; Roos, B. O.; Sadlej, A. J.; Wolinski, K. 2nd-order perturbation-theory with a CASSCF reference function. *J. Phys. Chem.* **1990**, *94*, 5483.

(50) Andersson, K.; Malmqvist, P. Å.; Roos, B. O. 2nd-order perturbation-theory with a complete active space self-consistent field reference function. *J. Chem. Phys.* **1992**, *96*, 1218.

(51) Finley, J.; Malmqvist, P.-Å.; Roos, B. O.; Serrano-Andrés, L. The multi-state CASPT2 method. *Chem. Phys. Lett.* **1998**, *288*, 299.

(52) Roos, B. r. O.; Malmqvist, P. k. Relativistic quantum chemistry: the multiconfigurational approach. *Phys. Chem. Chem. Phys.* **2004**, *6*, 2919.

(53) Malmqvist, P. Å.; Pierloot, K.; Shahi, A. R. M.; Cramer, C. J.; Gagliardi, L. The Restricted Active Space Followed by Second-Order

Perturbation Theory Method: Theory and Application to the Study of CuO2 and Cu2O2 Systems. *J. Chem. Phys.* **2008**, *128*, 204109.

(54) Sauri, V.; Serrano-Andrés, L.; Shahi, A. R. M.; Gagliardi, L.; Vancoillie, S.; Pierloot, K. Multiconfigurational Second-Order Perturbation Theory Restricted Active Space (RASPT2) Method for Electronic Excited States: A Benchmark Study. *J. Chem. Theory Comput.* **2011**, *7*, 153.

(55) Malmqvist, P. Å.; Roos, B. O.; Schimmelpfennig, B. The Restricted Active Space (RAS) State Interaction Approach with Spin-Orbit Coupling. *Chem. Phys. Lett.* **2002**, *357*, 230.

(56) Klooster, R.; Broer, R.; Filatov, M. Calculation of X-Ray Photoelectron Spectra With the Use of the Normalized Elimination of the Small Component Method. *Chem. Phys.* **2012**, *395*, 122.

(57) Griffith, J. S.; Orgel, L. E. Ligand-field theory. *Rev. Chem. Soc.* **1957**, *11*, 381.

(58) Robert, D. C. *The Theory of Atomic Structure and Spectra*; Los Alamos Series in Basic and Applied Sciences; University of California Press, 1981.

(59) Thole, B. T.; Cowan, R. D.; Sawatzky, G. A.; Fink, J.; Fuggle, J. C. New probe for the ground-state electronic structure of narrow-band and impurity systems. *Phys. Rev. B: Condens. Matter Mater. Phys.* **1985**, *31*, 6856.

(60) Okada, K.; Kotani, A.; Thole, B. T. Charge transfer satellites and multiplet splitting in X-ray photoemission spectra of late transition metal halides. *J. Electron Spectrosc. Relat. Phenom.* **1992**, *58*, 325.

(61) de Groot, F.; Kotani, A. *Core Level Spectroscopy of Solids*; CRC Press, 2008.

(62) de Groot, F. Multiplet effects in X-ray spectroscopy. *Coord. Chem. Rev.* **2005**, *249*, 31.

(63) Tanaka, A.; Jo, T. Resonant 3d, 3p and 3s photoemission in transition metal oxides pre- dicted at 2p threshold. *J. Phys. Soc. Jpn.* **1994**, *63*, 2788.

(64) Butler, P. H. *Point Group Symmetry Applications: Methods and Tables*; Plenum Press: New Yorka, 1981.

(65) Butorin, S. M. 3d-4f Resonant Inelastic X-ray Scattering of Actinide Dioxides: Crystal-Field Multiplet Description. *Inorg. Chem.* **2020**, *59*, 16251.

(66) van Besien, E.; Pierloot, K.; Görller-Walrand, C. Electronic spectra of uranyl chloride complexes in acetone: a CASSCF/CASPT2 investigation. *Phys. Chem. Chem. Phys.* **2006**, *8*, 4311−4319.

(67) Pierloot, K.; van Besien, E. Electronic structure and spectrum of UO22+and UO2Cl42−. *J. Chem. Phys.* **2005**, *123*, 204309.

(68) Zimmermann, P.; Hunault, M. O. J. Y.; de Groot, F. 1s2p RIXS calculations for 3d Transition Metal Ions in Octahedral Symmetry. *J. Spectrosc.* **2018**, *2018*, 3618463.

(69) Roos, B. O.; Lindh, R.; Malmqvist, P.-Å.; Veryazov, V.; Widmark, P.-O. Molecular dynamics simulations of the interactions between water and inorganic solids. *J. Phys. Chem. A* **2004**, *108*, 2851.

(70) Roos, B. O.; Lindh, R.; Malmqvist, P.-Å.; Veryazov, V.; Widmark, P.-O. New relativistic ANO basis sets for actinide atoms. *Chem. Phys. Lett.* **2005**, *409*, 295.

(71) Aquilante, F.; et al. MOLCAS 8: New Capabilities for Multiconfigurational Quantum Chemical Calculations across the Periodic Table. *J. Comp. Chem.* **2016**, *37*, 506.

(72) Roos, B. O. Chapter The mutliconfigurational (MC) Self-Consistent Field (SCF) Theory In *Lecture Notes in Quantum Chemistry*; Roos, B. O., Ed.; Springer: Berlin, Heidelberg, 1992.

(73) Khamesian, M.; Galván, I. F.; Delcey, M. G.; Sørensen, L. K.; Lindh, R. Spectroscopy of linear and circular polarized light with the exact semiclassical light−matter interaction. *Annu. Rep. Comput. Chem.* **2019**, *15*, 39.

(74) Autschbach, J. Orbitals for Analyzing Bonding and Magnetism of Heavy-Metal Complexes. *Comments Inorg. Chem.* **2016**, *36*, 215.

(75) Raboud, P.; Dousse, J.; Hoszowska, J.; Savoy, I. L₁ to N₅ atomic level widths of thorium and uranium as inferred from measurements of L and M x-ray spectra. *Phys. Rev. A* **1999**, *61*, 012507.

(76) Fuggle, J. C.; Alvarado, S. F. Core-level lifetimes as determined by x-ray photoelectron spectroscopy measurements. *Phys. Rev. A* **1980**, *22*, 1615.